SISSA

PAPER

Evaluation of depth-dose profiles in a water phantom at the BNCT facility at BINP

View the article online for updates and enhancements.
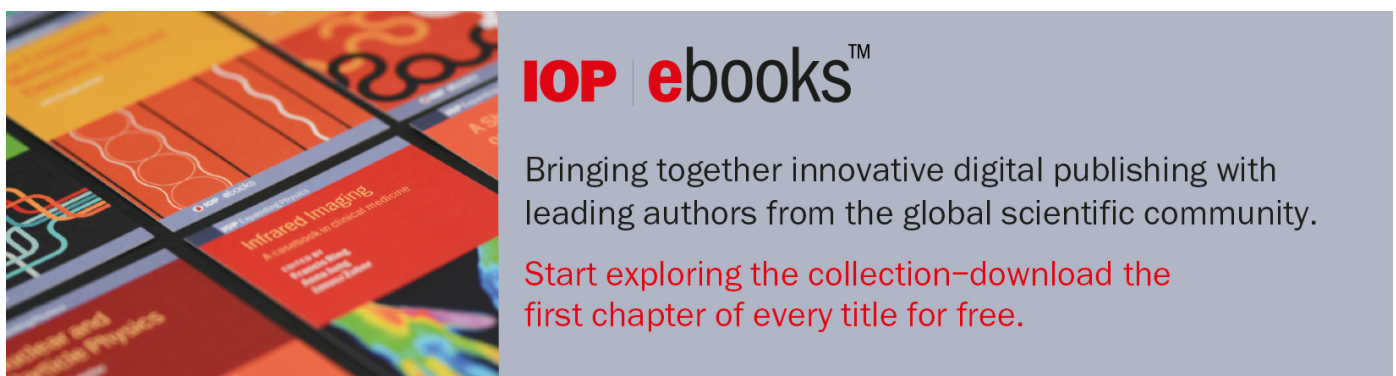
Evaluation of depth-dose profiles in a water phantom at the BNCT facility at BINP

T.A. Bykov,[a,b] **D.A. Kasatov,**[a,b] **A.M. Koshkarev,**[a,b] **A.N. Makarov,**[a,b] **V.V. Leonov,**[a]
V.V. Porosev,[a,b,*] **G.A. Savinov,**[a] **S.S. Savinov,**[a,b] **I.M. Shchudlo,**[a,b] **S.Yu. Taskaev**[a,b]
and G.D. Verkhovod[a,b]

[a]*Budker Institute of Nuclear Physics,*
Lavrentiev ave. 11, Novosibirsk 630090, Russia

[b]*Novosibirsk State University,*
Pirogova st. 2, Novosibirsk 630090, Russia

E-mail: porosev@inp.nsk.su

ABSTRACT: In this study, we present depth-dose profiles measured with a water phantom at the boron neutron-capture therapy (BNCT) facility at Budker Institute of Nuclear Physics (BINP). The presented results demonstrate that the proposed design of radiation detector with an optical fiber readout, which includes three different sensors (the first based on a plastic scintillator enriched with boron, the second based on a simple plastic scintillator, and the third having no scintillator at all), enables measurement of neutron flux, as well as estimations of the dose induced by gamma rays. The results of simulations with the GEANT4 package demonstrated good agreement with the experimental data and can be used for further system improvement.

*Corresponding author.

https://doi.org/10.1088/1748-0221/16/10/P10016

Contents

1   Introduction

Accelerator-based neutron sources are considered to be the most suitable option for pre-clinical and clinical studies for boron neutron-capture therapy (BNCT) [1]. Before a treatment, ^{10}B-enriched drugs are accumulated in the cancer cells, which become a target for the thermal neutrons. The ^{10}B$(n, \alpha)^7$Li reaction has two main channels, the products of which are $^7_3$Li$(1.02\,\text{MeV}) + \alpha(1.78\,\text{MeV}), 6\%$, and $^7_3$Li$(0.84\,\text{MeV}) + \alpha(1.47\,\text{MeV}) + \gamma(0.48\,\text{MeV}), 94\%$. In any case, the generated heavy particles liberate its energy within an area of a few tens of microns and effectively kill the cancer cells. For production of thermal and epithermal neutrons, a proton tandem accelerator with a lithium neutron-producing target was developed at BINP [2]. Evaluation of dose profiles obtained with the use of boron-enriched scintillators allows verifying the dose distributions in conditions similar to real treatment procedures. Besides neutrons, such systems generate a significant quantity of gamma rays. These gamma rays are associated both with the process of neutron generation on the lithium target [3] and with the reaction ^{1}H$(n, \gamma)^2$D [4]. Therefore, evaluation of the contribution of all possible components to the patient irradiation dose becomes a vital issue for treatment system optimization. To address this issue, we performed a series of experiments with a water phantom and a neutron flux monitoring system designed at BINP [5].

2   Water phantom experiment

To perform the measurements we manufactured a special water phantom. It was made from polycarbonate with a wall thickness of 8 mm. The internal volume of the phantom is $330 \times 313 \times 330\,\text{mm}^3$. The entry face of the phantom has a window made of PET plastic with a thickness of 0.5 mm. The control system, using stepper motors, is able to move a detector installed on a moving mechanism to any point in the water tank. In the experiments, the phantom was placed immediately behind the neutron-generating target. We used 3 detectors: *A*, *B*, and *C*. The detector *A* was located outside the water phantom, next to a stationary gamma radiation dosemeter, and its data were used for check of the stability of the monitoring system and cross-calibrations with the dosemeter. The
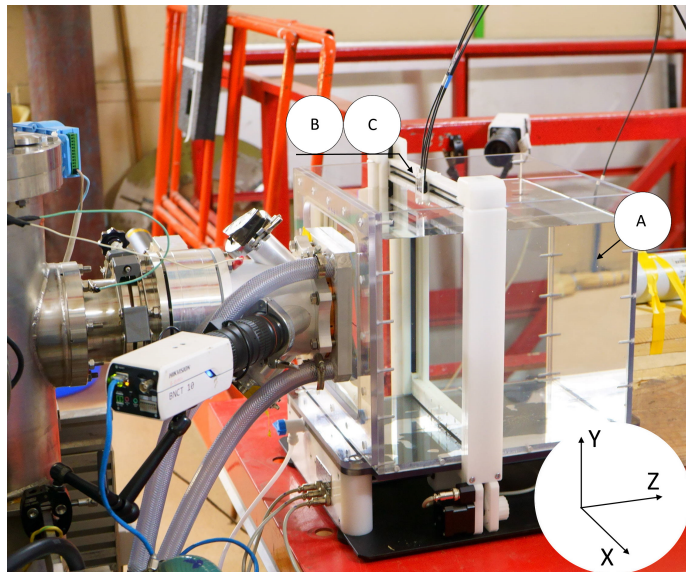
Figure 1. Experimental setup with water phantom installed immediately behind neutron-generating target. Arrows indicate position of detectors: *A* (behind water tank), *B*, and *C*.

detectors *B* and *C* were placed on the moving platform of the water phantom. Figure 1 demonstrates the experimental setup with the water phantom installed.

The detectors *A* and *B* had the same design, based on two different sensors [6]. The sensitive element of the sensors is a cylinder with a diameter of 1 mm and a length of 1 mm, made from plastic scintillator. In the sensors, we used polystyrene-based plastic scintillators produced in Russia (IHEP, Protvino [7]): SC-331, enriched with boron, further denoted as $B(n + \gamma + \text{Ch.})$, for the detector *B*, and SC-301, without boron, further denoted as $B(\gamma + \text{Ch.})$. The scintillation light from the sensors went by plastic optical fibers to the readout electronics and was detected by silicon photomultipliers (SiPMs) MPPC S13360-3050CS (HAMAMATSU). The electronics front-end is based on EASIROC ASIC [8], and pulses with an amplitude higher than a threshold were counted in the corresponding registration channels. For the noise rate of the SiPMs to decrease to a few Hertz, the temperature of the SiPMs was kept at 0°C. The difference in the counts of the two sensors allows us to estimate the contribution of the neutron component $B(n) = B(n + \gamma + \text{Ch.}) - B(\gamma + \text{Ch.})$, registered by the detector *B*.

The detector *C* has the same design, but it was specially produced without any scintillators. In fact, the data in the registration channels associated with the detector *C* were averaged for reduction of statistical fluctuations. The difference in the counts in the detector channel $B(\gamma + \text{Ch.})$ and the number of events registered by the detector $C(\text{Ch.})$, associated with the Cherenkov radiation generated in an optical fiber, yields a signal proportional to the dose of gamma radiation, $B(\gamma) = B(\gamma + \text{Ch.}) - C(\text{Ch.})$.

In the experiments, a proton beam with a diameter of ~ 10 mm was directed to the center of the lithium target. Figures 2, 3, and 4 demonstrate the measured event rate profiles along the *Z*- and *Y*-directions at different proton beam energies. The size of the error bars is compatible with the dot size. For convenience, the final data were recalculated for a proton beam current of 1 mA. The curve $B(\gamma + \text{Ch.})$ demonstrates the raw signal value in the registration channel with the boron-less scintillator in the detector *B*. The curve $B(n)$ demonstrates the restored count rate of

neutron capture events in the detector B. The curve $C(\text{Ch.})$ demonstrates the count rate of events induced by the Cherenkov light in the optical fibers. The curve $B(\gamma)$ demonstrates the restored count rate of gamma-related events in the detector B.
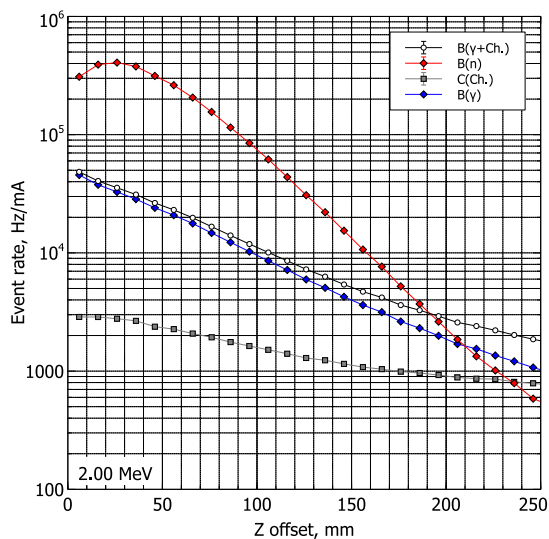

Figure 2. Event rate in detector channels vs. position along beam axis (Z-axis) in water phantom at proton beam energy of 2.00 MeV.
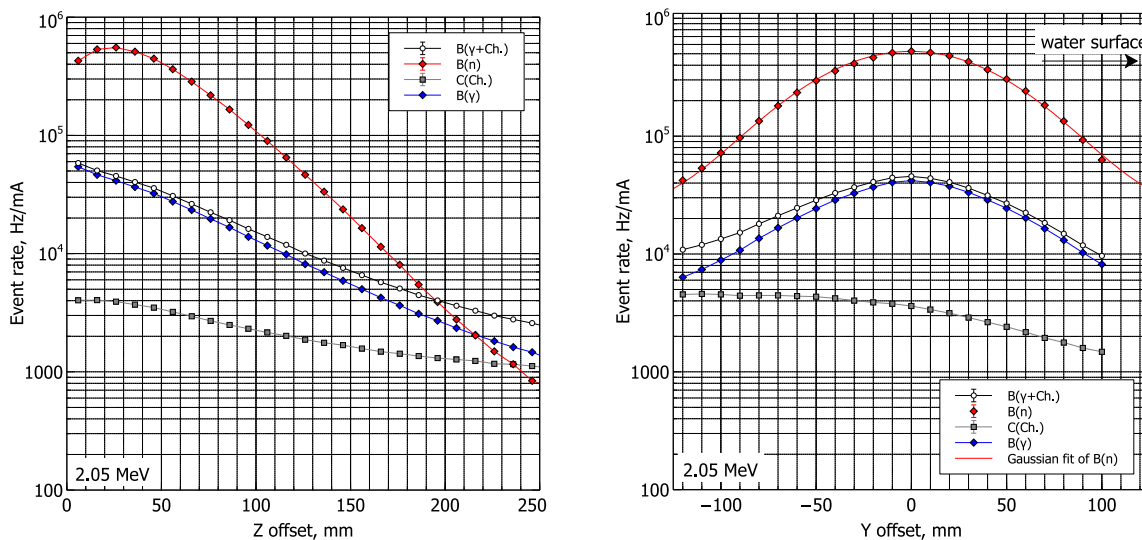

Figure 3. Event rate in detector channels along Z-axis (left) and along Y-axis near maximum of neutron dose (right) at proton beam energy of 2.05 MeV.

The asymmetry of the observed distributions along the Y-axis, measured with the detector C, is explained by the fact that the deeper the sensors went into the water phantom, the bigger part of optical fiber fell into the region with the maximum radiation intensity. It is seen that the three-sensor approach, when an additional scintillator-less registration channel measures the contribution of the Cherenkov light in a fiber, allows restoring the "true" symmetrical shape of gamma-related event
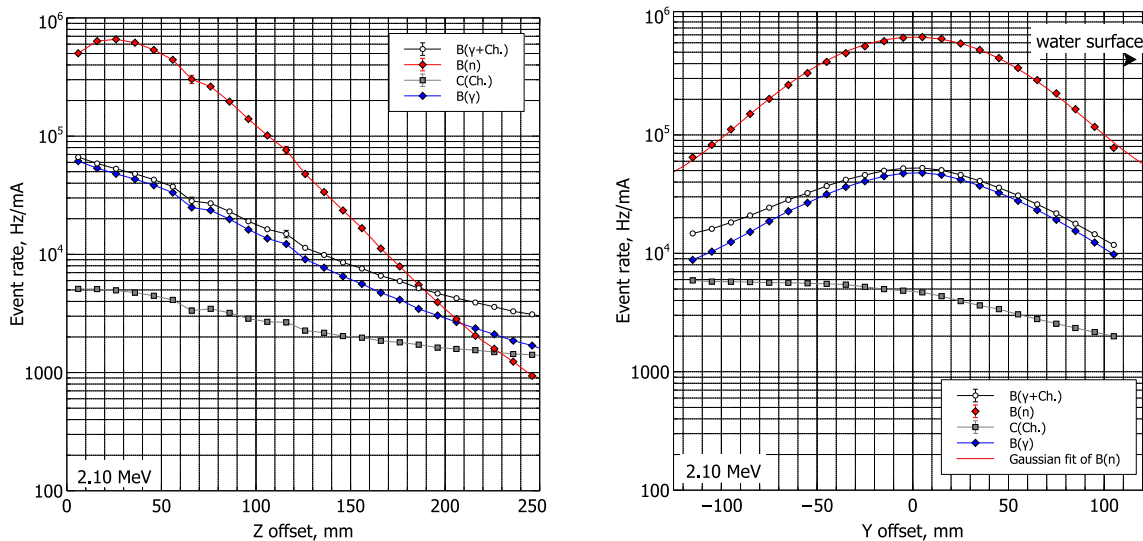
Figure 4. Event rate in detector channels along Z-axis (left) and along Y-axis near maximum of neutron dose (right) at proton beam energy of 2.10 MeV.

distributions in complex irradiation fields. Therefore, it becomes possible to estimate not only the dose absorbed due to boron capture, but the dose induced by photons too.

3 GEANT4 simulations

Monte-Carlo simulations are widely used for prediction of the behaviour of neutron generating facilities [9–12]. In our simulations, we applied the GEANT4 simulation package version 10.7.p01 [13]. This package traces every particle individually. On the one hand, it provides the most accurate results, and on the other hand, it requires a huge amount of computer resources. In the simulations, we used the HPE DL560 Gen10 server with four Intel Xeon Gold 6248 2500 MHz processors. To reduce the computation time we performed simulations as a two-step process. At the first stage, we generated 10^{11} protons in each run and calculated the spectra of neutrons that left the Li target towards the copper base. At that stage, we used the QGSP_BIC_AllHP physics list only, because it includes the low energy charged particle interaction based on the cross-section data taken from the ENDF/B-VII and the TENDL data libraries. In spite of the known limitations [14], it can provide resonable results [15–17] in our proton energy range. With the QGSP_BIC_HP physics list [18], generally recommended for medical applications, we did not observe correct generation of neutrons. The neutron-generating target was simulated with a series of layers made of natural Lithium with a thickness of 0.11 mm, copper basement with a thickness of 7 mm, cooling water with a thickness of 3 mm, and aluminum alloy (AMG5) with a thickness of 16.5 mm. Examples of the generated energy-angle distributions of neutrons are shown in figure 5. The shape of the observed distributions agrees with the expectations [19, 20].

At the second stage, we evaluated the depth-dose distributions in the geometry of a real experiment. In each run, we generated 10^9 neutrons in accordance with the previous energy-angle distributions. The initial positions of the primary particles relative to the beam axis followed a
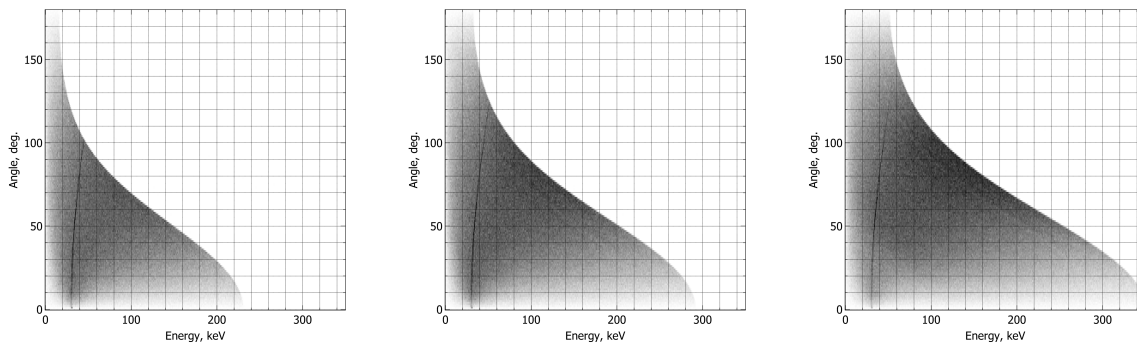
Figure 5. Angle-energy distribution of neutrons emitted from lithium target at proton beam energies of 2.00 MeV, 2.05 MeV, and 2.10 MeV.

Gaussian-like proton beam profile with a standard deviation of 5 mm in both directions [21]. The final data were rescaled to correspond to a proton beam current of 1 mA.

To estimate the detection rate in the Z-direction (parallel to the proton beam), we placed an array of detectors with a pitch of 1 cm in the water phantom. To estimate the dose distribution in the X-direction (perpendicular to the proton beam), we placed an array of detectors with a pitch of 1.5 cm at a Z-coordinate of 25 mm. Similar to the real experiments, each detector incorporated three sensors. The first one was based on the boron-enriched scintillator (SC-331), the second one was based on the boron-less scintillator (SC-301), and the last one, without any scintillator, was to detect the contribution of the Cherenkov light in an optical fiber. The length of plastic optical fibers in the simulations was 8.5 m, as in the real setup. The distributions of the number of detected optical photons for each detector (an example is shown in figure 6) were accumulated in each run and saved for further analysis.
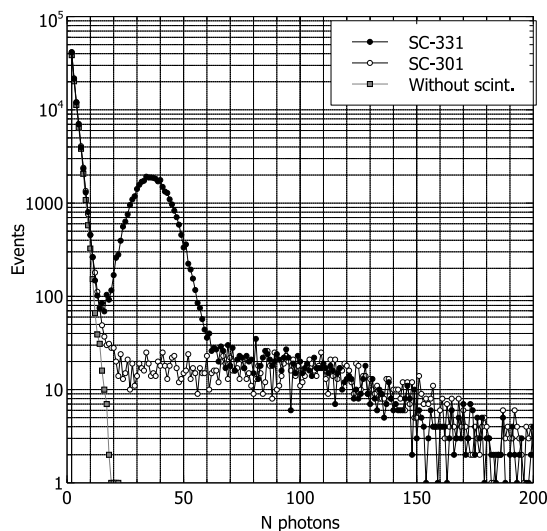

Figure 6. GEANT4 simulations of amplitude spectra in detector channels with different scintillators.

The results of simulations of the Z- and X-distributions at a detection threshold equal to 11 optical photons are shown in figures 7-9.
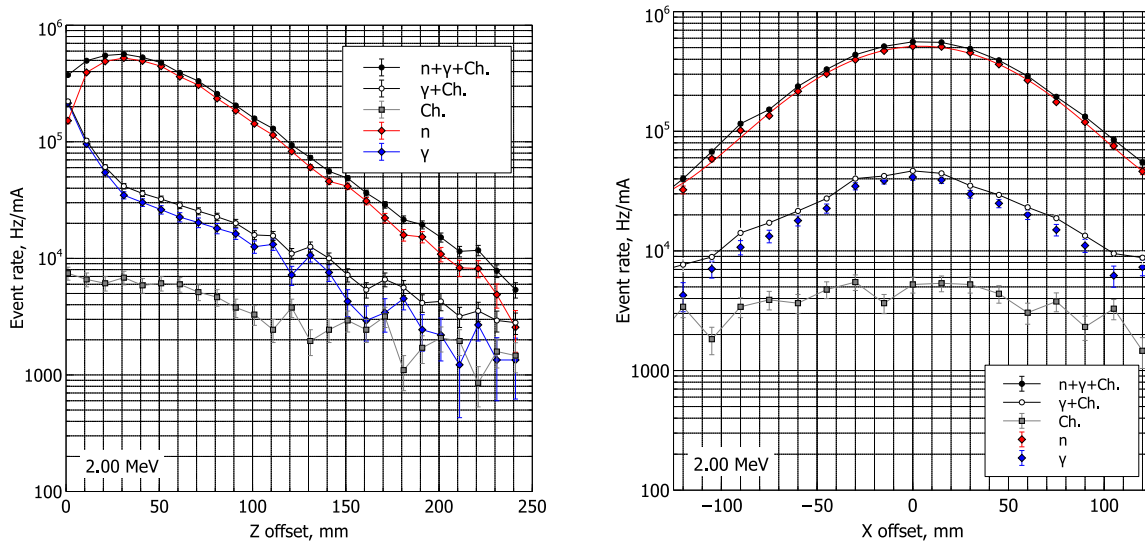
Figure 7. Event rate along *Z*-axis (left) and along *X*-axis near maximum of neutron dose (right) at proton beam energy of 2.00 MeV.
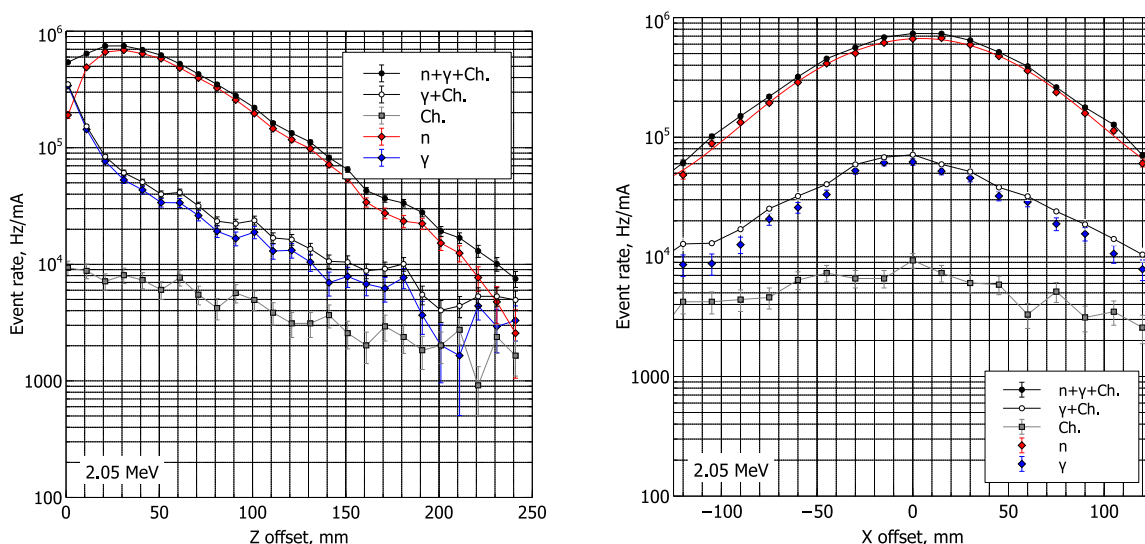

Figure 8. Event rate along *Z*-axis (left) and along *X*-axis near maximum of neutron dose (right) at proton beam energy of 2.05 MeV.

In this part of the simulations we compared different physics lists in GEANT4: "QGSP_BIC_HP" and "QGSP_BIC_AllHP" because it was known that different physics models could yield slightly different results [22]. Figure 10 demonstrates the maximum neutron rate as a function of the proton beam energy in the experiments and in simulations with different physics lists. Table 1 shows values of the parameter σ (standard deviation) of the Gaussian distributions fitting the distribution of neutron flux in the direction perpendicular to the particle beam in the position of the maximum dose.
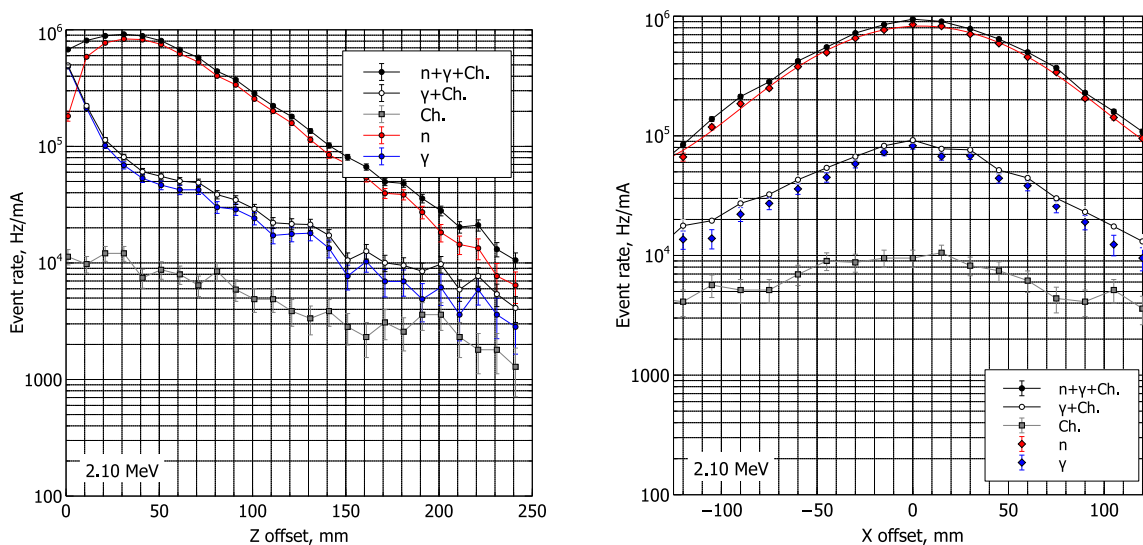
Figure 9. Event rate along *Z*-axis (left) and along *X*-axis near maximum of neutron dose (right) at proton beam energy of 2.10 MeV.

Table 1. Standard deviation (σ, mm) of Gaussian fit of neutron flux distribution in direction perpendicular to particle beam in position of maximum dose at different proton beam energies.

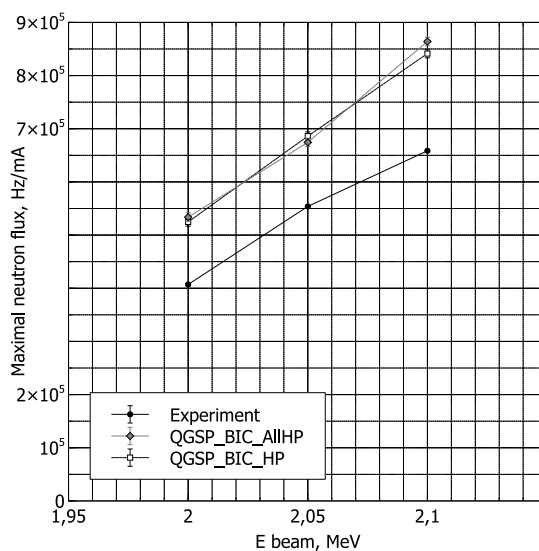|	2.00 MeV	2.05 MeV	2.10 MeV
QGSP_BIC_HP	46.7 ± 0.5	46.1 ± 0.6	48.6 ± 1.1
QGSP_BIC_AllHP	47.0 ± 0.5	48.1 ± 0.6	48.9 ± 0.7
Experiment	–	45.9 ± 0.1	46.8 ± 0.1

Figure 10. Maximum detected neutron flux vs. proton beam energy.

4 Results and discussion

It can be seen from the presented curves that the simulation results are in good agreement with the experiment. However, there is some shift of ≈ 4 mm in the Z-distributions in the simulations relative to the experimental data. One of the possible reasons may be the simplified geometric description of the complex internal water-cooling structure of the neutron-generating target in the simulations. In any case, it is necessary to carry out an experimental measurement of the real spectra of generated neurons to find out the true source of ambiguities. Additionally, we can see that the neutron count rate in the position of the maximum of the depth-dose curve in the simulations is bigger by 20% than the value obtained from the experimental data. There are few reasons for it. First, the real accelerator voltage, as followed from the calibration data, was less with a factor of 0.983 ± 0.001 than the actual one. Second, the actual diameter of the manufactured scintillators was in the range of 0.95–0.97 mm and it was less than 1 mm in the simulations. Another known feature of the setup is the non-perfect design of the sensors and the optical signal values lower than expected from the simulations. Therefore, some fraction of neutron-related events that produced a signal below a threshold could be missed. This issue is expected to be solved with a new sensor design based on quartz optical fibers with a significantly lower light attenuation. Another important source of bias is the uncertainty in the veritable boron concentration in the scintillators. This value is known from the manufacturer data only and should be verified with independent chemical analysis.

5 Conclusion

In this study, we tested the "three-sensor" approach to measuring the depth-dose distribution with a water phantom at the BNCT facility at BINP. The presented results show that the proposed system can be used for simultaneous monitoring of neutron and gamma fluxes. The application of SiPMs instead of vacuum photomultipliers dramatically simplified the design of the detection system and made it possible to realize a compact multichannel readout system. The results of simulations with the GEANT4 package demonstrated good agreement with the experimental data and can be used for further system improvement.

Acknowledgments

References

[1] Y. Kiyanagi, Y. Sakurai, H. Kumada and H. Tanaka, *Status of accelerator-based BNCT projects worldwide*, *AIP Conf. Proc.* **2160** (2019) 050012.

---

[1]http://nusc.nsu.ru.

[2] S. Taskaev, E. Berendeev, M. Bikchurina, T. Bykov, D. Kasatov, I. Kolesnikov et al., *Neutron source based on vacuum insulated tandem accelerator and lithium target*, *Biology* **10** (2021) 350.

[3] S. Taskaev, T. Bykov, D. Kasatov, I. Kolesnikov, A. Koshkarev, A. Makarov et al., *Measurement of the $^7Li(p,p'\gamma)^7Li$ reaction cross-section and 478 keV photon yield from a thick lithium target at proton energies from 0.65 MeV to 2.225 MeV*, *Nucl. Instrum. Meth. B* **502** (2021) 85.

[4] T. Kobayashi, Y. Sakurai and M. Ishikawa, *A noninvasive dose estimation system for clinical BNCT based on PG-SPECT-conceptual study and fundamental experiments using HPGe and CdTe semiconductor detectors*, *Med. Phys.* **27** (2000) 2124.

[5] T.A. Bykov et al., *A multichannel neutron flux monitoring system for a boron neutron capture therapy facility.*, 2019 *JINST* **14** P12002.

[6] T.A. Bykov et al., *Initial trials of a dose monitoring detector for boron neutron capture therapy*, 2021 *JINST* **16** P01024.

[7] V. Rykalin, V. Brekhovskikh, S. Chernichenko, A. Gorin and V. Semenov, *Development of the polystyrene scintillator technology and particle detectors on their base*, *J. Phys. Sci. Appl.* **5** (2015) 6.

[8] S. Callier, C.D. Taille, G. Martin-Chassard and L. Raux, *EASIROC, an easy & versatile ReadOut device for SiPM*, *Phys. Procedia* **37** (2012) 1569.

[9] S.A. Darda, A.Y. Soliman, M.S. Aljohani and N. Xoubi, *Technical feasibility study of BAEC TRIGA reactor (BTRR) as a neutron source for BNCT using OpenMC monte carlo code*, *Prog. Nucl. Energy* **126** (2020) 103418.

[10] K.W. Van Delinder, R. Khan and J.L. Gräfe, *Neutron activation of gadolinium for ion therapy: a monte carlo study of charged particle beams*, *Sci. Rept.* 10 (2020) 1.

[11] K. Tanaka, T. Kobayashi, Y. Sakurai, Y. Nakagawa, M. Ishikawa and M. Hoshi, *The benchmark of the simulation calculation for near-threshold $^7Li(p,n)^7Be$ reaction in neutron capture therapy*, *J. Nucl. Sci. Technol.* **39** (1992) 1290.

[12] L. Moghaddasi and E. Bezak, *Development of an integrated monte carlo model for glioblastoma multiforme treated with boron neutron capture therapy*, *Sci. Rept.* **7** (2017) 7069.

[13] J. Allison et al., *Recent developments in Geant4*, *Nucl. Instrum. Meth. A* **835** (2016) 186.

[14] D. Cano-Ott, E. Mendoza and P. Arce, *Open questions about the G4ParticleHP model*, [https://indico.cern.ch/event/434968/contributions/1933074/attachments/1174289/1696816/Considerations_about_G4ParticleHP.pdf].

[15] T. Amin, A. Infantino, R. Barlow and C. Hoehr, *Validating production of PET radionuclides in solid and liquid targets:Comparing Geant4 predictions with FLUKA and measurements*, *Appl. Radiat. Isot.* **133** (2018) 61.

[16] F. Tabbakh and N.S. Hosmane, *Enhancement of radiation effectiveness in proton therapy: Comparison between fusion and fission methods and further approaches*, *Sci. Rept.* **10** (2020) 5466.

[17] Y. Lu, Z. Xu, L. Zhang, Z. Wang, T. Li and M.S. Khan, *GEANT4 simulations of the neutron beam characteristics for 9be/7li targets bombarded by the low energy protons*, *Nucl. Instrum. Meth. B* **506** (2021) 8.

[18] P. Arce, D. Bolst, M.-C. Bordage, J.M.C. Brown, P. Cirrone, M.A. Cortés-Giraldo et al., *Report on G4-Med, a Geant4 benchmarking system for medical physics applications developed by the Geant4 medical simulation benchmarking group*, *Med. Phys.* **48** (2021) 19.

[19] C.L. Lee and X.-L. Zhou, *Thick target neutron yields for the $^7Li(p,n)^7Be$ reaction near threshold*, *Nucl. Instrum. Meth. B* **152** (1999) 1.

[20] C.L. Lee, *The design of an intense accelerator-based epithermal neutron beam prototype for BNCT using near-threshold reactions*, Ph.D. Thesis, Massachusetts Institute of Technology, Department of Nuclear Engineering, (1998) [http://hdl.handle.net/1721.1/50535].

[21] A. Badrutdinov, T. Bykov, S. Gromilov, Y. Higashi, D. Kasatov, I. Kolesnikov et al., *In situ observations of blistering of a metal irradiated with 2-MeV protons*, *Metals* **7** (2017) 558.

[22] Z. Chen, P. Yang, Q. Lei, Y. Wen, D. He, Z. Wu et al., *Comparison of BNCT dosimetry calculations using different GEANT4 physics lists*, *Radiat. Prot. Dosim.* **187** (2019) 88.